



Modelling of concrete at early ages: Application to an externally restrained slab

Rui Faria ^{*}, Miguel Azenha, Joaquim A. Figueiras

Faculdade de Engenharia da Universidade do Porto, Rua Dr. Roberto Frias s/n, 4200-465 Porto, Portugal

Received 16 May 2005; accepted 1 February 2006

Available online 6 May 2006

Abstract

In view of the growing use of High Performance Concrete, with large hydration-induced volumetric changes (both thermal and shrinkage related), numerical modelling of concrete at early ages has become an important issue, regarding the possible formation of cracks, with undesirable consequences on aesthetics and structural durability. In this paper a thermo-mechanical model based on the framework of finite element techniques is presented, and involves the consideration of phenomena such as the heat production induced by the cement hydration, the evolving properties of concrete during hydration and early-age creep. A numerical application is presented, focused on the thermo-mechanical behaviour of a slab strongly restrained by the supporting piles, which has been monitored during the construction phase. For this particular problem it is shown that by making a reasonable thermal and mechanical characterization of concrete, the thermo-mechanical model provides results that are well correlated with the observed in situ measurements, namely the temperatures and the strains.

© 2006 Elsevier Ltd. All rights reserved.

Keywords: Cement hydration; Thermo-mechanical behaviour; Early-age; Ageing; Creep; Numerical modelling

1. Introduction

The early-age behaviour of concrete structures has proved to be an important issue with regard to many practical situations. In fact, at early ages, thermal stresses that develop as a consequence of cement hydration can cause the evolving concrete tensile strength to be reached, and cracks to appear. These cracks are usually classified in two categories [1]: the ‘surface cracks’, reaching depths, roughly saying, of about a few centimetres from the concrete faces, and the ‘through cracks’, when discontinuities cross the entire concrete section.

Surface cracks are generated during the heating phase of the cement hydration reaction, and may close during the subsequent cooling phase. This kind of cracks may have some visual impact, constituting an entry doorway for external aggressive agents, affecting concrete durability.

On the other hand, through cracks occur when the contraction of concrete during the cooling phase is internally or externally restrained, and they affect durability and eventually structural stability as they introduce strong discontinuities.

Bearing in mind the increasing use of High Performance Concrete (HPC), with heat of hydration potentials and autogenous shrinkage greater than Normal Strength Concrete (NSC), and the generalized awareness of the importance of durability issues, considerable efforts have been made to predict (and if possible to avoid) the above-mentioned cracks. Many researchers [2–7] have proposed different approaches for reproducing numerically the early-age concrete performance. In this paper, a thermo-mechanical numerical strategy for analysing the early-age concrete behaviour is described, allowing the best decisions about the concrete composition, the construction phasing and the curing techniques to be adopted, or the most appropriate scheduling for the prestressing operations. Such a numerical procedure is devised for a Finite Element (FE)

^{*} Corresponding author. Tel.: +35 122 508 1950; fax: +35 122 508 1835.

E-mail address: raria@fe.up.pt (R. Faria).

implementation, and it includes a thermal model that accounts for the heat generation due to cement hydration, and a mechanical model for computing strains and stresses.

Thermal and mechanical effects are coupled, in the sense that thermal phenomena influence mechanical behaviour, and vice-versa:

- (i) Mechanical behaviour is influenced by the thermal field primarily because thermal changes cause concrete to expand and contract; if these volumetric changes are restrained, thermal stresses will arise. On the other hand the thermal field influences the hydration kinetics, which directly affects the evolution of the concrete mechanical properties, and consequently the evolution of stresses (with possible formation of cracks).
- (ii) Even though less important, the influence of the mechanical behaviour on the thermal field also exists: upon concrete cracking, a discontinuity is created, affecting transmission of heat; furthermore, concrete expansion or contraction may induce losses of contact with the formwork, leading to changes in the thermal boundary conditions.

The coupling of the thermo-mechanical problem, dealt with in the bi-directional format just described, renders quite costly calculations, regarding the many interdependencies and nonlinearities involved. Accordingly, and bearing in mind that the thermal field is only marginally affected by the mechanical one, it is usual to consider a unidirectional coupling in which the mechanical analyses are performed after the thermal computations, receiving from the latter the distributions of temperature and degree of hydration. With such an option, also adopted here, the thermal problem is assumed independent from the mechanical one, a simplifying rule consensually assumed as reasonably accurate [8].

Therefore, a typical thermo-mechanical analysis starts by fitting a FE mesh to the concrete structure, the nodal temperatures of which are computed during time by solving the thermal problem engendered by the heat released during the cement hydration reaction. A normalized variable termed ‘hydration degree’ is adopted to monitor the degree of completion of the cement hydration, and the rate of heat production during this reaction, strongly dependent on the local temperature, is ruled by the Arrhenius law. These matters concerned with the thermal problem are the scope of Section 2 of the present paper.

With the field of temperatures computed for each time step, the inherent volumetric changes lead to strains that are computed on a mechanical problem with proper allowance for the external and internal restraints, as well as to shrinkage and creep phenomena, the latter reproduced with the Double Power Law and adopting a Taylor’s expansion of the hierarchical integral of strains. Evolution of the concrete mechanical properties is reproduced through an ageing model where the enhancement of the

concrete strengths and the Young’s modulus are functions of the hydration degree. Section 3 is concerned with the relevant aspects of the mechanical problem. Through an algorithm-like flowchart, the chain of operations that are required to perform a thermo-mechanical analysis is outlined at the end of this section.

In Section 4, the application of the described methodology to a slab supported on a regular mesh of piles is detailed. This slab, in regard to the strong restraints induced by the piles, is quite suitable for the validation purposes, and it was monitored during the early ages.

2. Thermal problem

2.1. Fourier’s law and internal heat generation

The thermodynamic equilibrium of a concrete domain under thermal transient conditions is expressed by the Fourier’s law

$$k \nabla \cdot (\nabla T) + \dot{Q} = \rho c \dot{T} \quad (1)$$

where k is the thermal conductivity, T is the temperature, \dot{Q} is the rate of internal heat generated by the cement hydration and ρc is the volumetric specific heat.

Regarding the characterization of k and ρc , one should be aware of their evolution during the cement hydration process. The experimental determination of these properties is usually performed with laboratory procedures, such as the Guarded Hot Plate [9] or the Two Linear Parallel Probe methods [10]. Analytical predictions of these properties can also be made based upon a weighted average of the thermal properties of the mixture components (see [11] for details).

Thermal conductivity k of the hardened concrete is known to be strongly dependent on the kind of aggregates used in the mixture, and it usually ranges between 1.2 and 3.5 W/m °C [12]. During cement hydration thermal conductivity endures significant changes, and there is experimental evidence that in the first hours after mixing thermal conductivity is about 20–30% greater than in hardened concrete; according to Ruiz et al. [13] the concrete thermal conductivity can be considered to vary according to

$$k = k_\infty (1.33 - 0.33\alpha) \quad (2)$$

where k_∞ stands for the value of thermal conductivity for hardened concrete, and the hydration degree α quantifies the extent of the cement hydration reaction already undertaken (for civil engineering applications the hydration degree is usually computed as the ratio between the heat released up to a certain instant t and the total heat expected at completion of the cement hydration reaction [14]).

In what concerns the specific heat of concrete ρc , it has a relatively constant value along the cement hydration reaction, exhibiting variations below 5% of its final value (see bibliographic review in De Schutter [15]). Therefore, it is feasible to adopt a constant value for this thermal property,

matching the hardened concrete specific heat, which typically ranges between 800 and 1170 J/kg °C [16,17].

As far as the hydration heat production is concerned, experimental evidence shows that higher temperatures engender faster cement hydration reactions, the kinetics of which being then reproduced by an Arrhenius law of the form [18]

$$\dot{Q} = af(\alpha)e^{-\frac{E_a}{RT}} \quad (3)$$

where E_a is the activation energy (J/mol), R is the universal gas constant (8.314 J/mol K⁻¹), a is the maximum value of the heat production rate (J/s) and $f(\alpha)$ describes the evolution of the normalized heat production rate as a function of the hydration degree α . Eq. (3) can also be expressed in the form $\dot{Q} = a\dot{\alpha}$, since the rate evolution of the hydration degree is in fact

$$\dot{\alpha} = f(\alpha)e^{-\frac{E_a}{RT}} \quad (4)$$

Eq. (3) can be directly calibrated from an adiabatic experimental test of the concrete mixture (which provides the $T-t$ curve, where t denotes time), or indirectly through other calorimetric techniques, like semi-adiabatic or isothermal tests [19,20]. Alternatively, parameters and the function $f(\alpha)$ involved in Eq. (3) can be obtained from analytical approaches or micro-structural models specifically devised to reproduce the cement hydration, namely the Hymostruc [14], the Multi-Component Hydration [21] or the CHEMY3D [22], among others.

Regarding the activation energy, the most efficient and accurate experimental procedure to quantify it for use in Eq. (3) is through isothermal calorimetry [23]. Nevertheless, the following reference values may be used for the Arrhenius constant E_a/R in Portland cements [19,24]:

$$\frac{E_a}{R}(K) = \begin{cases} 4000, & T \geq 20^\circ C \\ 4000 + 175(20 - T), & T < 20^\circ C \end{cases} \quad (5)$$

2.2. Boundary conditions

As far as the boundary conditions of the thermal problem are concerned, the convection and radiation phenomena are of relevance for the analysis of early-age concrete. Convection refers to the heat transfer that occurs between the concrete surface and a moving fluid (usually the air), when a temperature gradient is installed between both materials. According to the Newton's cooling law [25] the convective heat transfer can be expressed as

$$q = h_c(T_s - T_a) \quad (6)$$

where q is the convective heat flux per unit area, h_c is the convection coefficient, T_s and T_a are the surface and the air temperatures (K), respectively. Based on the wind speed v (m/s), the convection coefficient may be estimated as follows [6]:

$$h_c = \begin{cases} 5.6 + 3.95v, & v \leq 5 \text{ m/s} \\ 7.6v^{0.78}, & v > 5 \text{ m/s} \end{cases} \quad (7)$$

Radiation is related to the heat transfer between two bodies at different temperatures, for instance between the concrete and the air. The heat exchange between concrete and the environment due to radiation can be expressed according to the Stefan–Boltzmann equation in the following way [25]:

$$q_r = \varepsilon\sigma(T_s^4 - T_a^4) \quad (8)$$

where ε is the emissivity of concrete (usually within the range 0.85–0.95) and σ is the Stefan–Boltzmann constant [$\sim 5.67 \times 10^{-8} \text{ W m}^{-2} \text{ K}^{-4}$].

For simplicity radiation is usually accounted for together with convection, through a single convection–radiation coefficient $h_{cr} = h_c + h_r$, where [17,26].

$$h_r = \begin{cases} \varepsilon[4.8 + 0.075(T_a - 278.15)], & T_a \geq 278.15 \text{ K} \\ 4.8\varepsilon, & T_a < 278.15 \text{ K} \end{cases} \quad (9)$$

(This simplification is valid for the usual range of temperature differences between concrete surfaces and the environment.)

The convection–radiation coefficient is applicable under the hypothesis of direct contact between the concrete's surface and the air. In practical situations, where complex scaffold conditions and temporary curing covers are frequently encountered, an 'equivalent heat transfer coefficient' h_{eq} is usually preferred to be applied in Eq. (6). The many material layers existing between the concrete surface and the air may be viewed as associated in series, and accordingly one may compute the equivalent boundary coefficient as

$$h_{eq} = \left(\frac{1}{h_{cr}A} + \sum_1^n \frac{L_i}{k_i A} \right)^{-1} \quad (10)$$

where A is the unit area through which heat transfer is occurring, and for each i th layer L_i is the thickness and k_i is the conduction coefficient.

Heat transfer to concrete due to solar radiation can be accounted for through simple multiplication of the incident solar energy by the solar absorvity of the concrete surface (usually ~ 0.65). The prediction of the incident radiation is possible by the use of relatively simple models [27] that account for factors such as the orientation of the surface, latitude, shadow cast by neighbouring objects, cloudiness of the sky, disturbance of the atmosphere, etc. Such models were not used in the present research, as the concerned application was cast indoors.

2.3. Implementation via the FE method

Following standard procedures in the FE method, and assuming the usual interpolation strategy $T = NT^e$, where N denotes the interpolation matrix and T^e designates the nodal temperatures for a given FE with volume Ω , the weak form for the thermal equations (accounting for the convection/radiation Newman conditions in boundary

Γ_q , and assuming that \mathbf{N} trivially fulfils the Dirichlet conditions) becomes

$$\begin{aligned} \int_{\Omega} \mathbf{N}^T \rho c \dot{T} d\Omega + \int_{\Omega} \nabla \mathbf{N}^T k \nabla T d\Omega \\ = \int_{\Omega} \mathbf{N}^T \dot{Q} d\Omega - \int_{\Gamma_q} \mathbf{N}^T q d\Gamma_q \end{aligned} \quad (11)$$

Writing this equation for time t_{n+1} , and assuming a backward-Euler integration scheme of the form

$$\dot{T}_{n+1} = (T_{n+1} - T_n)/\Delta t \quad (12)$$

with Δt being the interval between time steps t_n and t_{n+1} , Eq. (11) leads to the following equation, suitable for computational implementation:

$$\frac{1}{\Delta t} \mathbf{C}^e (\mathbf{T}_{n+1}^e - \mathbf{T}_n^e) + \mathbf{H}^e \mathbf{T}_{n+1}^e = \mathbf{F}_T^e + \mathbf{F}_Q^e \quad (13)$$

where the elemental matrices and ‘force vectors’ (referenced by index ‘e’) are computed in accordance to Eqs. (11) and (12), rendering

$$\mathbf{C}^e = \int_{\Omega} \mathbf{N}^T \rho c \mathbf{N} d\Omega \quad (14)$$

$$\mathbf{H}^e = \int_{\Omega} \nabla \mathbf{N}^T k \nabla \mathbf{N} d\Omega + \int_{\Gamma_q} \mathbf{N}^T h \mathbf{N} d\Gamma_q \quad (15)$$

$$\mathbf{F}_T^e = \int_{\Gamma_q} \mathbf{N}^T h_{eq} T_A d\Gamma_q \quad (16)$$

$$\mathbf{F}_Q^e = \int_{\Omega} \mathbf{N}^T \dot{Q}_{n+1} d\Omega \quad (17)$$

Standard assembling procedures can now be invoked to constitute the global \mathbf{C} and \mathbf{H} matrices and the \mathbf{F}_T and \mathbf{F}_Q vectors required for the FE analysis of a structural problem, that is,

$$\left(\frac{\mathbf{C}}{\Delta t} + \mathbf{H} \right) \mathbf{T}_{n+1} = \mathbf{F}_T + \mathbf{F}_Q + \frac{\mathbf{C}}{\Delta t} \mathbf{T}_n \quad (18)$$

Due to the dependency of the hydration heat rate on the temperature, expressed in Eq. (3), \mathbf{F}_Q is nonlinearly dependent on \mathbf{T}_{n+1} . Accordingly, an incremental-iterative procedure supported by the Newton–Raphson method is usually adopted to solve Eq. (18), towards extracting the nodal temperatures \mathbf{T}_{n+1} [28].

3. Mechanical problem

3.1. Overview

In order to evaluate the strains and stresses that develop in concrete at the local level, the thermal model described in Section 2 has to be complemented with a mechanical model. With enough accuracy the thermal problem can be solved before the mechanical one, since the evolution of the hydration reaction is practically independent of the strains and stresses that develop in concrete. As far as the mechanical model is concerned, it can only be activated after the thermal model, from which it receives the local

temperatures indispensable for computing the volumetric strains $\varepsilon_T = \alpha_T T \mathbf{1}$, where α_T is the thermal dilation coefficient and $\mathbf{1}$ is the unit tensor.

Furthermore, and regarding the viscous nature of concrete during hydration, the mechanical model should account for the creep, which plays a crucial role in the development of stresses (either due to thermal effects, volumetric deformations or external actions). In fact, creep deformation of concrete at early ages may lead to stress fluctuations that reach magnitudes of 50% or higher [29], as will be illustrated in the application at the end of this paper. A key point also concerned with this matter is that the progression of the hydration reaction makes the concrete properties (particularly the elastic modulus and the compressive and tensile strengths) to be dynamic, and accordingly an aging model is needed to appropriately evaluate the cracking risk.

In HPC autogenous shrinkage is also a matter of concern at early ages, since the volume of the solids being formed as a result of the cement hydration reaction is less than the sum of the volumes of the concrete mix components, which at a macroscopic standpoint leads to contraction of the concrete during the early ages. This peculiar phenomenon is essentially a direct consequence of the reduced water-to-cement ratios adopted in HPC, contrarily to what occurs in NSC, where the water content is higher than the one necessary to ensure full hydration of cement. As a consequence of these dissimilar situations, in NSC drying shrinkage is far more important than autogenous shrinkage [30], and conversely it occurs in HPC. Within the ‘time window’ concerned with early age concrete proper allowance to shrinkage phenomenon is therefore essential when dealing with HPC, usually reproduced numerically by prescribing a dynamic volumetric contraction, cumulative to the volumetric variations induced by the thermal problem ε_T , and accounting for creep as well. The application of Section 4 is concerned with NSC, and consequently shrinkage was disregarded, as autogenous shrinkage was not important and drying shrinkage is not of relevance during the early ages.

3.2. Ageing

Phenomenologically the growth of concrete mechanical properties during hydration is linked to the hydration degree α , as this entity may be viewed as an indicator of how much the inherent chemical reaction has already advanced. From a mechanical point of view some initial threshold of the hydration degree exists, up to which concrete mechanical properties are negligible. This initial hydration degree α_0 is related to the instant at which the concrete mixture undergoes the transition from a suspension to a solid [31], and accordingly only when $\alpha > \alpha_0$ is the concrete considered to have a solid skeleton. Determination of such initial hydration degree is still a controversial matter, as different assessment methods may lead to different values of α_0 : some authors recommend that it

should be obtained through Vicat needle tests [32], but suggestions to adopt ultrasonic measurements [33] or electrical testing (among others) are also encountered.

Based on the experimental results, the following relations were established by Rostásy et al. [34] for the compressive strength f_c , the tensile strength f_t , and the Young's modulus E_c of concrete, based on the hypothetical end values obtained by regression for these mechanical properties at $\alpha = 1$, here termed f_{cl} , f_{tl} and E_{cl}

$$f_c(\alpha) = f_{cl} \left(\frac{\alpha - \alpha_0}{1 - \alpha_0} \right)^{3/2} \quad (19)$$

$$f_t(\alpha) = f_{tl} \left(\frac{\alpha - \alpha_0}{1 - \alpha_0} \right) \quad (20)$$

$$E_c(\alpha) = E_{cl} \left(\frac{\alpha - \alpha_0}{1 - \alpha_0} \right)^{1/2} \quad (21)$$

Obviously, the use of these equations does not necessarily imply that $\alpha = 1$ is reached. In fact, final values of degree of hydration lower than 1 have been reported for mixes with $w/c < 0.36$ [35].

In what concerns the thermal dilation coefficient α_T and the Poisson's ratio, they are both considered here to be constant throughout hydration as long as $\alpha > \alpha_0$, with the typical values usually considered for hardened concrete, that is, $\alpha_T = 10 \times 10^{-6} \text{ }^{\circ}\text{C}^{-1}$ and $v = 0.2$, respectively [36].

3.3. Creep

As stated before, creep deformation of concrete is of uttermost importance at early ages, and consequently mechanical analyses must include a creep model to allow for realistic predictions of the strain and stress fields, leading to credible cracking risk estimations. In this approach only basic creep is considered, as during early ages drying creep can only be observed near the concrete surfaces (1–2 cm deep), therefore with marginal influence [34].

To account for the basic creep at time t a compliance function $J(t, t')$ is adopted in the present paper, where t' is the instant of loading. Accordingly the strain tensor $\varepsilon(t, t')$ is computed as

$$\varepsilon(t, t') = \int_0^t J(t, t') d\sigma(t') + \varepsilon_0(t) \quad (22)$$

where $\sigma(t')$ is the stress tensor applied at time t' , and $\varepsilon_0(t)$ is the stress independent strain tensor linked to the thermal and shrinkage phenomena (that is, $\varepsilon_0 = (\alpha_T T + \varepsilon_S)1$, with ε_S being the shrinkage deformation). The most widely used function for describing the early-age creep, providing good predictions [37], is the Double Power Law (DPL) [38]

$$J(t, t') = \frac{1}{E_0} + \frac{\phi_1}{E_0} (t')^{-m} (t - t')^n \quad (23)$$

where E_0 is the asymptotic elastic modulus (corresponding to short term loads), and ϕ_1 , m and n are material parameters.

Because of the large stress fluctuations that occur in concrete during the early ages, the DPL is implemented numerically on a time step transient analysis by approximating Eqs. (22) and (23) with a Taylor series expansion [8], instead of the customary practice adopted in the modelling of creep in hardened concrete, based on a Dirichlet expansion. The use of a Taylor series preserves the well-known interesting features of a Dirichlet expansion, that is, the possibility to express the stress tensor increment $\Delta\sigma$ as an explicit function of the strain tensor increment $\Delta\varepsilon$ by involving state variables that are continuously updated at each time step, which accounts for the previous stress and strain histories (see [8] for details). This ensures a quite efficient numerical algorithm and circumvents the computationally cumbersome need for storing the stress and strain histories throughout the entire analysis, as would be necessary with a direct implementation of Eq. (22).

3.4. Outline of the thermo-mechanical analysis

A brief outline of the overall procedure for a thermo-mechanical analysis is illustrated in Box 1, where the most relevant operations needed for evaluating the final stress tensor are reproduced.

Box 1. Outline of the thermo-mechanical analysis

Thermal problem

- (i) Initialize time step counter: $n = 0$.
- (ii) Set $n = n + 1$ and update current time: $t_{n+1} = t_n + \Delta t$.
Is $t_{n+1} > t_{end}$? NO: Go to step (iii).
YES: Go to step (viii).
- (iii) Initialize iteration counter: $i = 0$.
Initialize variables $T_{n+1}^{i=0} = T_n$ and $\alpha_{n+1}^{i=0} = \alpha_n$.
- (iv) Set $i = i + 1$.
- (v) Set $\mathbf{T}_{n+1}^i = \mathbf{T}_{n+1}^{i-1}$ and $\alpha_{n+1}^i = \alpha_{n+1}^{i-1}$.
Compute $(\mathbf{F}_T)_{n+1}^i$ according to Eq. (16).
Compute $\mathcal{Q}_{n+1}^i(T_{n+1}^i, \alpha_{n+1}^i)$ according to Eq. (3), and evaluate $(\mathbf{F}_Q)_{n+1}^i$ according to Eq. (17).
- (vi) Solve Eq. (18) for \mathbf{T}_{n+1}^i .
Discretize Eq. (4) as $(\alpha_{n+1}^i - \alpha_n)/\Delta t = f(\alpha_{n+1}^i) \times \exp(-E_a/(RT_{n+1}^i))$, and solve through the Newton–Raphson method to extract α_{n+1}^i .
- (vii) Compute norms $\|\mathbf{T}_{n+1}^i\|$ and $\|\alpha_{n+1}^i\|$. Is convergence achieved?
NO: Go to step (iv).
YES: Go to step (ii).

Mechanical problem

- (viii) Reinitialize time step counter: $n = 0$.
Initialize the displacement vector $\mathbf{a}_n = \mathbf{0}$.
- (ix) Set $n = n + 1$ and update current time: $t_{n+1} = t_n + \Delta t$.

- Is $t_{n+1} > t_{\text{end}}$? NO: Go to step (x).
YES: Stop.
- (x) Get \mathbf{T}_{n+1} and α_{n+1} from the thermal analysis database.
Update concrete properties according to the current hydration degree: $E_{c_{n+1}}(\alpha_{n+1})$, $f_{t_{n+1}}(\alpha_{n+1})$, $f_{c_{n+1}}(\alpha_{n+1})$.
 - (xi) Update the elasticity matrix $\mathbf{D}_{n+1}(E_{c_{n+1}}, v)$, form the FE stiffness matrix $\mathbf{K}_{n+1}^e = \int_{\Omega} \mathbf{B}^T \mathbf{D}_{n+1} \mathbf{B} d\Omega$ and compute the FE incremental force vector $\Delta \mathbf{f}_{n+1}^e$.
 - (xii) Assemble contributions from all the FE, and solve the mechanical problem $\mathbf{K}_{n+1} \Delta \mathbf{a}_{n+1} = \Delta \mathbf{f}_{n+1}$ for the incremental displacement vector $\Delta \mathbf{a}_{n+1}$.
 - (xiii) Update the displacement vector $\mathbf{a}_{n+1} = \mathbf{a}_n + \Delta \mathbf{a}_{n+1}$.
Compute strains at each Gauss point: $\varepsilon_{n+1} = \mathbf{B} \mathbf{a}_{n+1}$.
Compute stresses at each Gauss point, with allowance to thermal and creep deformations $\sigma_{n+1} = \sigma_{n+1}(\mathbf{D}_{n+1}, \varepsilon_{n+1}, T_{n+1})$.
 - (xiv) Check cracking risk at each Gauss point.

4. Application: slab strongly restrained by the supporting piles

4.1. Overview

The numerical strategy described above for reproducing the early-age behaviour of concrete structures will be illustrated in this application, which concerns a reinforced concrete floor slab of a robotized milk storage building, with very tight constraints in regard to the differential vertical deflections under service loads. The slab is 143 m long, 41 m wide and 0.35 m thick, supported on piles arranged on a $3 \times 4 \text{ m}^2$ mesh, and reinforced on each face and both directions with $\varnothing 16 \text{ mm}$ rebars spaced at 0.15 m (see Figs. 1 and 2). The piles restrain significantly the free expansion or contraction of the slab (Fig. 1b details the slab–pile connection), and since special performance requirements hindered the using of structural joints, the present application is quite prone to early-age cracking, and therefore suitable for numerical validation.

Fig. 3 reproduces the sequence of construction adopted for concreting the slab via longitudinal and transverse strips, cast at the specified dates. For the intended purposes of validation some points of a 6 m wide strip concreted at 07/04/2003 were monitored during the first days after casting (see Fig. 3), to measure the concrete strains (along direction X in location “ \times ” and direction Y in location “ $+$ ”) and temperatures. In Fig. 4a two pairs of strain/temperature sensor heads are visible at location “ \times ”: one on the bottom layer of reinforcement and one on the top layer,

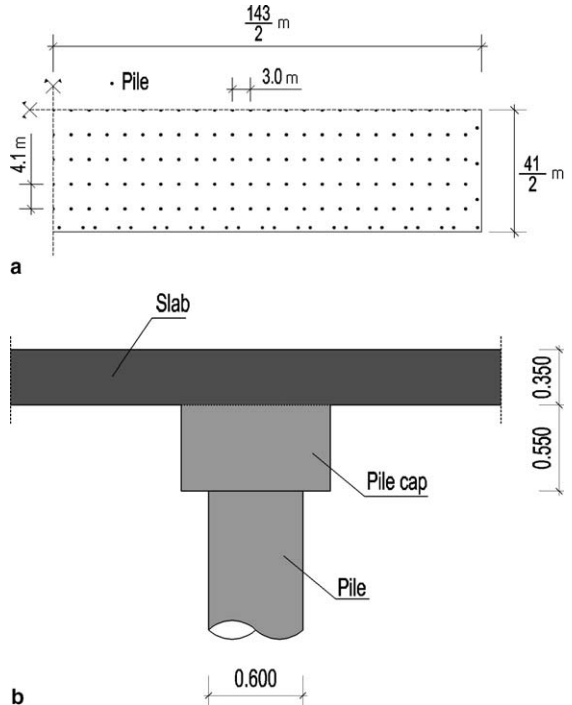


Fig. 1. Analysed slab: (a) structural plan; (b) slab–pile connection.



Fig. 2. Overall view of slab reinforcement ($\# \varnothing 16 \text{ mm}/0.15 \text{ m}$).

and both 5 cm from the outer slab surfaces. Each sensor head consists of a $\varnothing 10 \text{ mm}$ non-ribbed bar, with approximately 800 mm between two welded plate anchorages (see detail in Fig. 4b), on the central part of which an electrical strain gauge and a thermal sensor are fixed. With this sensor holder an average strain on the 800 mm length is expected to be measured, in an attempt to reduce local disturbances due to concrete cracking. The environmental temperature around the monitored slab strip was also recorded with a thermal sensor.

No specific thermal or mechanical laboratory characterization tests of the concrete were available. Therefore, regarding such scarce information, several simplified and exploratory analyses will be presented first using 1D and 2D idealizations, and only at the end a refined 3D simulation will be performed. Besides, influence of reinforcement

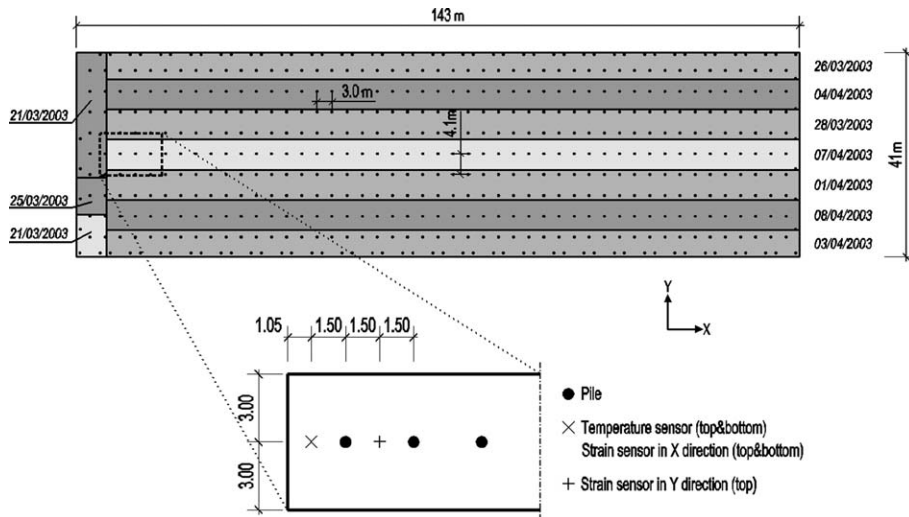


Fig. 3. Sequence of construction and monitored strip (cast on 07/04/2003).

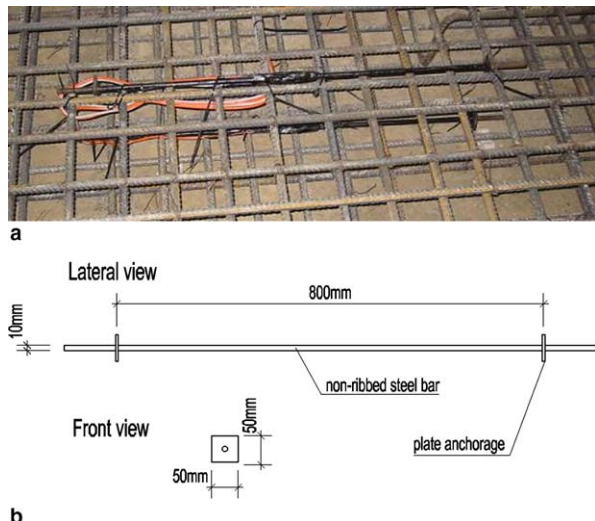


Fig. 4. Sensors in X direction at “ x ” position: (a) temperature and strain sensors; (b) geometry outline of the sensor.

was not accounted for, since at present time very limited research can be found on this subject in regards to structural concrete at early ages [1].

Since a laboratory adiabatic $T-t$ curve was not available for characterizing the heat generation potential of the concrete used in the slab, based on the known chemical composition of the cement and on the cement content of the mixture (285 kg/m^3) a pseudo characterization curve was computed via the above referred Multi-Component Hydration model [21], and it is reproduced in Fig. 5. Average values for the thermal conductivity and the specific heat of the concrete were assumed in all the analyses, as well as for the activation energy [39] – see details in Table 1.

4.2. 1D model

First thermal analyses of the monitored strip were made under the assumption that heat transfer with the neigh-

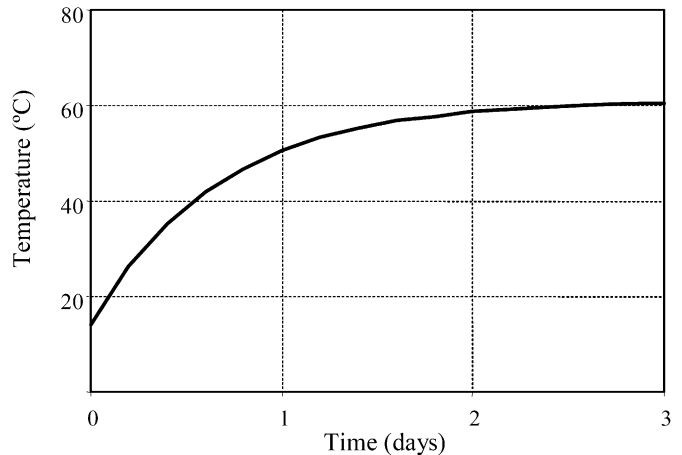


Fig. 5. Pseudo-adiabatic characterization curve.

Table 1

Thermal properties of concrete and boundary conditions

Concrete thermal conductivity	$k = 2.6 \text{ W/mK}$
Concrete volumetric specific heat	$\rho_c = 2400 \text{ J/m}^3\text{K}$
Convection coefficient in boundary P1–P2	$h = 4.5 \text{ W/m}^2\text{K}$
Convection coefficient in boundary P3–P4	$h = 7.5 \text{ W/m}^2\text{K}$
Temperature of soil	17°C
Activation energy	$E_a = 50 \text{ kJ/mol}$

bouring environment could only occur across the slab thickness (in other words: negligible heat transfer is assumed parallel to the slab middle plane). Hence, such simplified analysis results in a 1D heat transfer problem along the normal Z to the slab, as schematized in Fig. 6.

The air temperatures registered throughout the monitoring campaign were considered on the upper boundary of the FE model. A far more realistic simulation should also account for the soil below the concrete slab, bringing the necessity of a thermal characterization of the former, which was not available. Therefore, a simplified convective

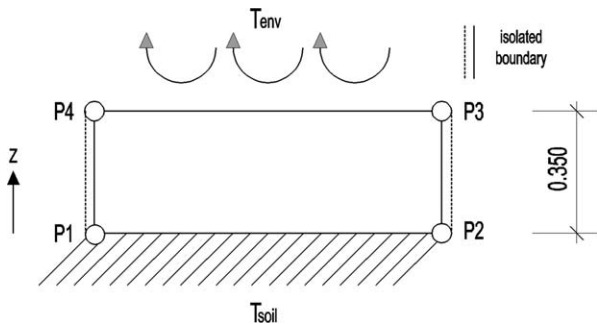


Fig. 6. Geometry of the 1D simplified model.

boundary between the slab and the soil was considered, supported by the following strategy:

- First, and based on the estimated wind speed for the site, an average value for the convection coefficient in the slab-air interface (boundary P3–P4 in Fig. 6) was computed with Eq. (7).
- Then, the convection coefficient and the soil temperature (assumed as constant) to be stipulated at P1–P2 boundary of Fig. 6 were searched via a trial-and-error procedure, oriented towards making the computed temperatures during the cooling phase match the temperature evolution registered in the monitoring campaign, and particularly the daily thermal variations evident in Fig. 7 after 5 days, as the latter correspond to a thermal equilibrium with the environment that is independent from the concrete heating/cooling phase. The final data obtained from this strategy are summarized in Table 1.

The thermal analyses were performed on a mesh with 7 quadrilateral FE along direction Z , integrated with 2×2 Lobatto points, and extended for a period of 9.2 days with time steps of 1 h. Results concerning the evolution of temperatures in two points on the upper and bottom reinforcement layers are depicted in Fig. 7, and compared with measurements from the experimental campaign. Having in mind the adopted simplifications and the crude thermal characterization of the materials involved, there is a fairly good coherence between the numerical and the experimental results. The observed deviations are thought to be mainly caused by two reasons: (i) on one hand the inactivity period at the beginning of hydration was not correctly reproduced, leading to differences during the heating phase, and (ii) on the other hand the simplified assumptions made for defining both the upper and lower boundary convection coefficients for the slab, namely in what concerns the P1–P2 boundary, and the fact that the P3–P4 boundary did not account for a provisional textile that covered the slab during the first 24 h.

In Fig. 8, evolutions of temperature and hydration degree are presented for the two points located on the upper and lower reinforcement layers, as well as for a point

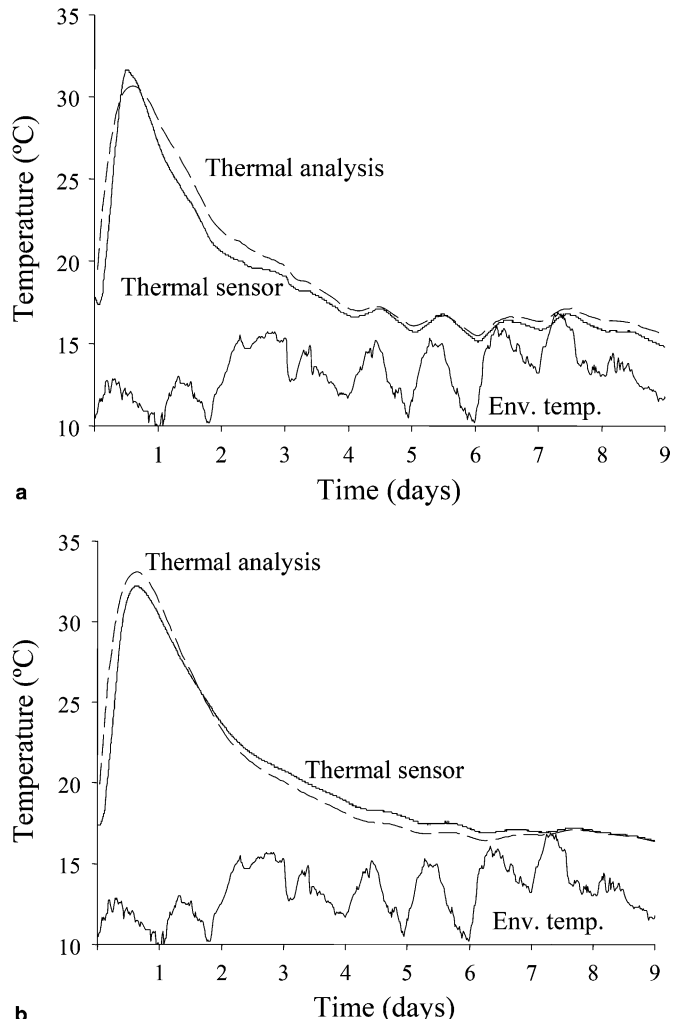


Fig. 7. Temperature evolutions in two points: (a) 5 cm from the top; (b) 5 cm from the bottom.

on the slab middle plane. According to Fig. 8a the temperature gradient across the thickness is quite low, with a maximum of only 4 °C; accordingly in Fig. 8b the hydration degree exhibits also a quite homogenous evolution across the thickness, and hence the same is expected to occur with the concrete mechanical properties.

In what concerns the mechanical analysis that was performed thereafter, and based on the specified concrete class, the mechanical properties shown in Table 2 were used. The FE mesh was identical to the one adopted for the thermal analysis, but 8-noded Serendipity elements with a 2×2 Gauss-Legendre integration quadrature were preferred for the mechanical analysis. Fig. 9a reproduces the evolution of the in-plane normal stresses for the above referred three points across the thickness. As expected, since the slab is restrained stresses are compressive during the heating phase, and start diminishing during the cooling phase, until tensile stresses are reached. A mechanical analysis without consideration of creep is depicted in Fig. 9b, to illustrate how the normal stresses and their evolutions are

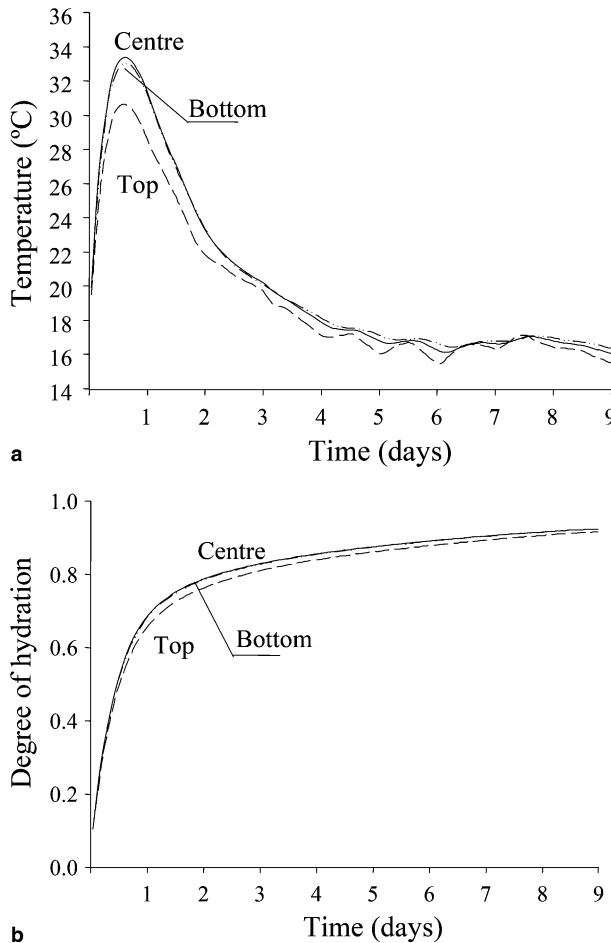


Fig. 8. Results from the thermal analysis: (a) temperature; (b) hydration degree.

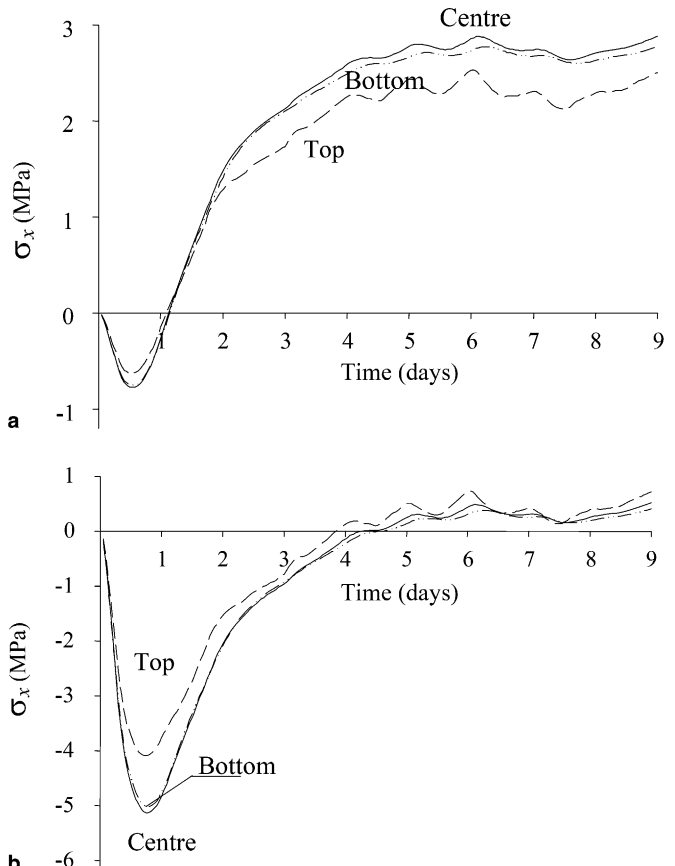


Fig. 9. Results from the mechanical analysis: (a) with creep; (b) without creep.

4.3. 2D model

Taking into consideration the 1D results just presented, the implications of the phasing adopted for the strip casting were analysed with a 2D model that discretizes the slab middle plane. The evolutions of the temperature and hydration degree at each point on the central plane, idealized as representative of all points along the corresponding normal, are assumed to coincide with the ones obtained with the 1D model. This simplification, equivalent to neglecting any heat transfer in the plane of the slab, was also adopted by Gutsch [5]. For the present strictly mechanical analysis the strip cast in 07/04/2003 was selected, represented in Fig. 10 by the ‘hardening concrete’ domain.

Besides this simplification the following further ones were also considered:

- Only a 30 m long and 6 m wide hardening concrete strip was assumed as representative of the real one with $6 \times 137 \text{ m}^2$ in plan, to reduce the computational cost of the analyses. Around this strip contour P1–P2–P5–P4–P8–P6 of Fig. 10 (‘hardened concrete’) was included to reproduce the effect of the concrete slab already hardened.
- Supporting piles were considered to act horizontally as rigid supports on their insertion points into the slab middle plane.

Table 2
Mechanical properties of concrete

Young's modulus	$E_c = 29 \times 10^9 \times \alpha^{0.5} \text{ Pa}$
Poisson's ratio	$\nu = 0.2$
Expected compressive strength	$f_{c1} = 38 \text{ MPa}$
Expected tensile strength	$f_{t1} = 2.9 \text{ MPa}$
Thermal dilation coefficient	$\alpha_T = 10 \times 10^{-6} \text{ K}^{-1}$
Creep law parameters (DPL)	$\phi_1 = 2.26; m = 0.35; n = 0.3$

dissimilar from the ones reproduced in Fig. 9a. This illustrates the extreme importance of creep in concrete early-age performance, since by disregarding this phenomenon one might have concluded that tensile stresses would never reach 1 MPa, which is an unsafe conclusion in comparison to the values of about 3 MPa predicted when creep is accounted for. This points out an important conclusion, which contradicts some engineering common sense: creep does not always provide reduction of the undesirable tensile stresses, since as it also attenuates the growth of compressive stresses during the heating phase (compare Fig. 9a and b up to 1 day), the subsequent incursion into tension during the cooling phase is inherently aggravated.

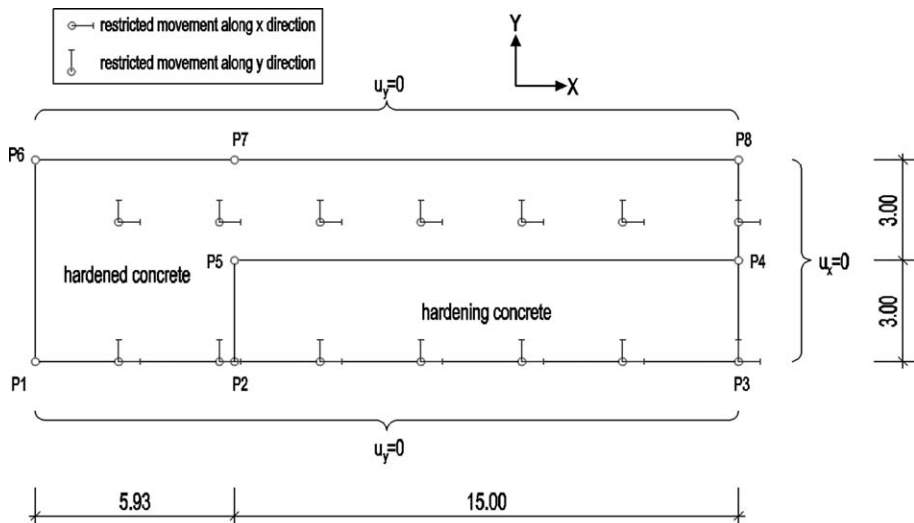


Fig. 10. Geometry of the slab middle plane.

- Friction between the lower surface of the slab and the soil was neglected.
- Axes P1–P3 and P6–P8 in Fig. 10 are assumed as planes of symmetry.
- Perfect bond is considered between the young and the hardened concrete interfaces.
- Hardened concrete was assumed without temperature changes during the analyses, and with a 100% hydration degree.

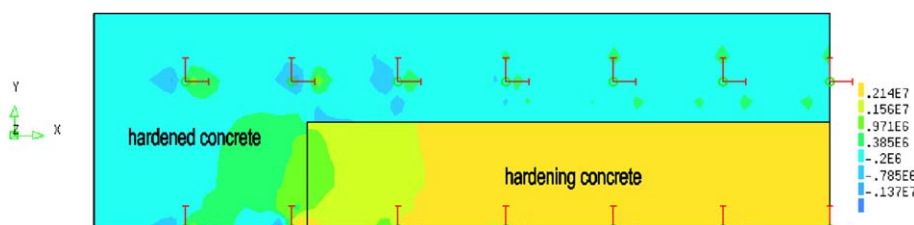
Mechanical properties of the concrete are the same as already listed in Table 2. The adopted FE mesh is quite refined and regular, constituted by a total of 340 finite elements with 8 nodes, integrated with 2×2 Gauss points. For the transient analysis the same strategy mentioned for the 1D model was pursued.

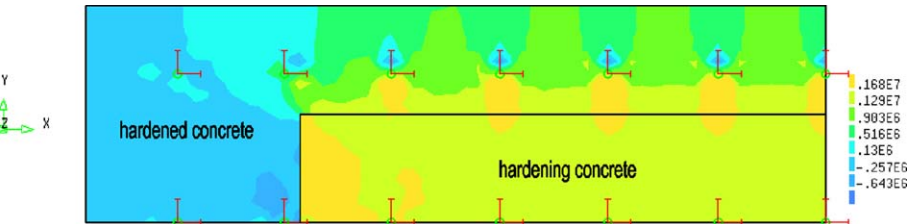
In terms of results, attention is drawn to the normal stresses along the X and Y directions depicted in Figs. 11 and 12 for the instant $t = 9.2$ days, when maximum tensile stresses were detected in Fig. 9. Stresses σ_x in the hardening concrete strip vary from 0.9 MPa close to line P2–P5 up to 2.5 MPa near contour P3–P4, this latter value being about 86% of the 2.9 MPa reported for the ‘infinite slab’ assumed in Fig. 9. Regarding the normal stresses σ_y , peak values in the hardening concrete (approximately 2 MPa) occur near line P2–P5, where the hardened concrete provides significant restriction. Taking into consideration the used con-

crete class as C30/37, according to Eurocode 2 [36] the average tensile strength should be 2.9 MPa at the age of 28 days, which according to the above reported normal stresses computed for the slab leads to the conclusion that transverse cracking should be expected. On-site inspection of the slab confirmed this prediction, since a repetitive pattern of cracks normal to the X direction were found, as illustrated in Fig. 13. The width of these cracks is obviously controlled by the reinforcement, in conformity to what was expected in design, but the good correlation between the orientation really observed for the cracks and the numerical predictions is remarked here as an overall validation of the numerical model and the pursued simulation strategies.

4.4. 3D model

To confirm the validity of the previous two combined simplified models, a 3D thermo-mechanical analysis was performed. The corresponding 3D FE mesh included 4 finite elements across the thickness (direction Z), and in plane XY the same discretization as for the 2D model was adopted: thus, a total of 3×340 FE was considered. Prismatic 8-noded elements with a $2 \times 2 \times 2$ Lobatto integration scheme were adopted for the thermal analysis, whereas for the mechanical analysis 20-noded elements with $3 \times 3 \times 3$ Gauss points were considered. All thermal

Fig. 11. Normal stresses (Pa) along direction X ($t = 9.2$ days).

Fig. 12. Normal stresses (Pa) along direction Y ($t = 9.2$ days).Fig. 13. Cracking pattern parallel to direction Y .

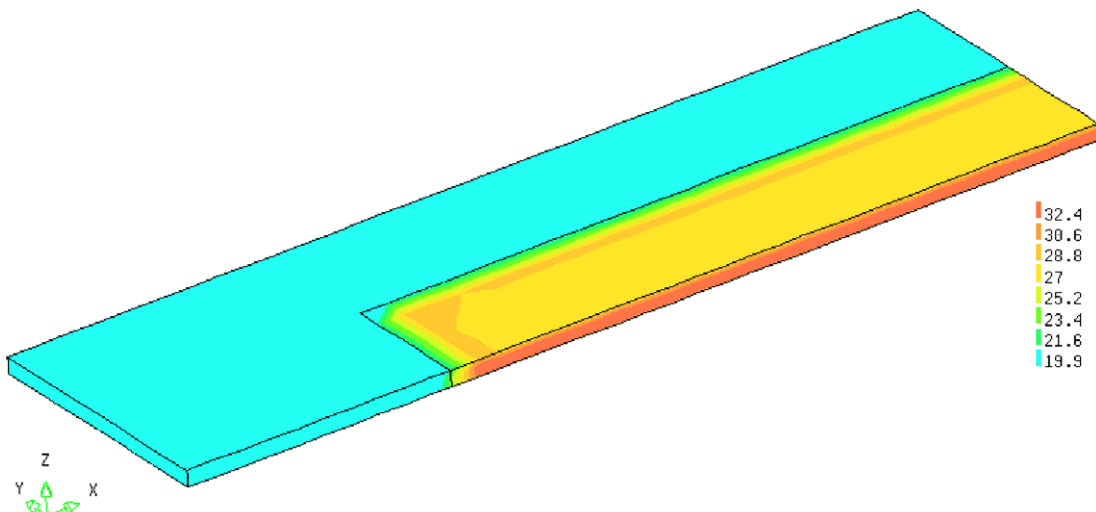
properties concerning the ‘hardening concrete’ are the same as for the 1D model, whereas for the ‘hardened concrete’ they correspond to full hydration. Vertical boundaries parallel to planes XZ and YZ were defined as thermally isolated along the normal direction, and in the ‘hardened concrete’ temperature was assumed to coincide with the environmental one measured experimentally. As regards to the mechanical restrictions, in the symmetry planes normal displacements were prevented; in the connection of the slab to the piles all displacement components were restricted; and all nodes of the bottom plane of the slab were assumed with null vertical displacements.

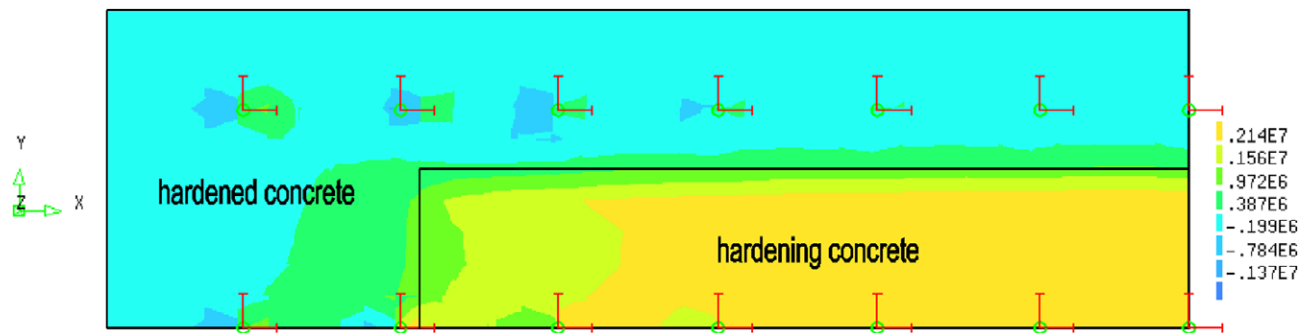
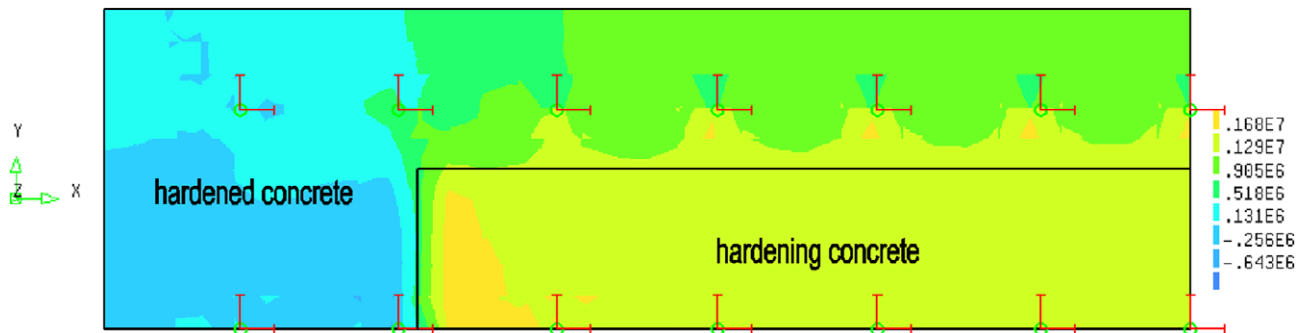
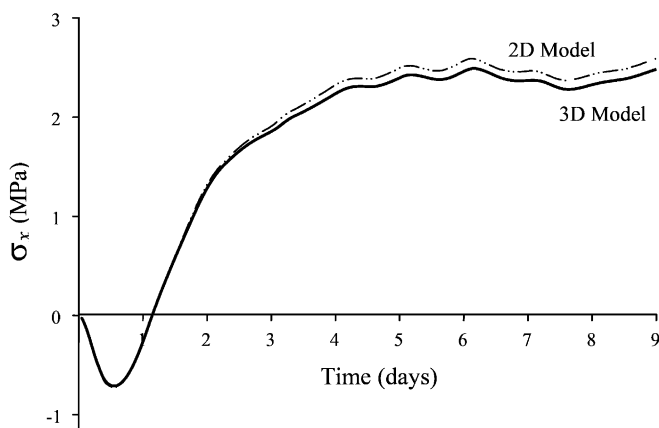
Concerning the thermal analysis, the first conclusion to be outlined from inspection of Fig. 14 is that the simplifica-

tion adopted for the 1D model, according to which the thermal flux was assumed to occur essentially along the vertical direction Z , was quite close to reality: in this figure the predicted thermal field at $t = 1$ day is almost homogeneous in both the ‘hardening’ and ‘hardened’ concrete domains, and only minor heat conduction effects are perceptible on their interfaces. At point “ \times ” (see Fig. 3), at a distance of 1 m from the interface between the two concrete domains, agreement between the temperatures obtained with the present 3D model and the ones reported for the 1D analysis is almost perfect, with an irrelevant deviation of about 2%.

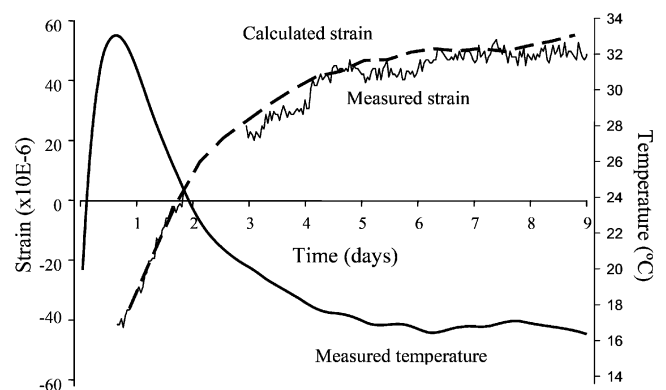
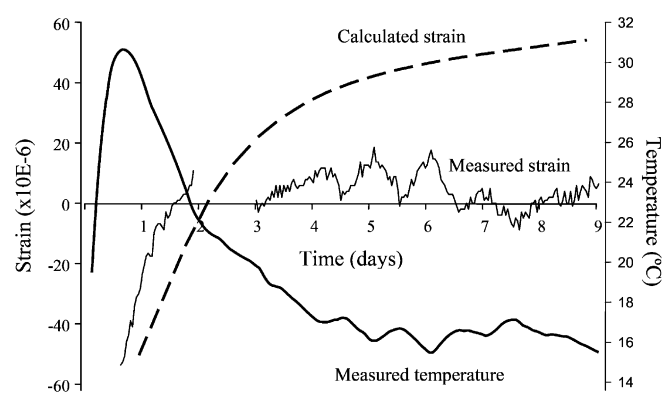
Regarding the mechanical results with the 3D model, stresses σ_x and σ_y on the slab middle plane generally match the ones obtained with the 2D model, as it can be realized by comparing Figs. 15 and 16 with Figs. 11 and 12. This consistency of the stress predictions from the 3D and 2D numerical models is even further emphasized in Fig. 17, where evolutions of σ_x at the critical point P3 of Fig. 10 are compared for both idealizations: it can be noted that stress differences are rather small, below 5%.

The present 3D model allows the strains predicted numerically to be compared against the ones obtained during the in-field monitoring campaign. A prior call of attention is yet drawn to the great difficulty in defining the precise instant at which a strain sensor is effectively bonded to concrete undergoing hydration, and becomes 100%

Fig. 14. Temperature ($^{\circ}$ C) at $t = 1$ day.

Fig. 15. Normal stresses (Pa) along direction X , at middle plane ($t = 9.2$ days).Fig. 16. Normal stresses (Pa) along direction Y , at middle plane ($t = 9.2$ days).Fig. 17. Normal stresses along direction X in point P3.

operational to measure the concrete strains. A reasonable assumption is needed to define this instant, and accordingly we will assume here that full bond of the sensor unit to the concrete is expected to occur when concrete starts cooling. Having in mind these considerations, two strain evolutions will be discussed for a pair of sensors indicated in Fig. 3: the ones concerning the “ \times ” bottom sensor and the “ $+$ ” top sensor, reproduced in Figs. 18 and 19, respectively. In Fig. 18 the temperature evolution at “ \times ” bottom sensor allows one to define the onset of the cooling phase, after which comparison of the numerical and experimental strains along direction X is pertinent: as it can be observed, both the magnitude and the development through time of

Fig. 18. Strains along direction X at bottom sensor in “ \times ”.Fig. 19. Strains along direction Y at top sensor in “ $+$ ”.

the numerical strain after the peak temperature agree fairly well with the measured ones. It is noteworthy to mention that due to an electrical disturbance in the construction site, strain gage data between the second and third days was lost, and thus it is not plotted in Figs. 18 and 19.

In Fig. 19 a similar comparison is presented for the strains along direction Y at “+” top sensor, but in this case the agreement between the numerical and the experimental evolutions is only reasonable up to $t = 2$ days, being clearly worse thereafter due to an unexpected trend of the monitored strain curve, which oscillates with the daily temperature variations, but does not grow as concrete contracts during the cooling phase. A possible explanation for this behaviour could be the formation of concrete cracks near the sensor's anchor plates, but outside the sensor length, which could have caused the sensor to loose mechanical restriction, and the concrete strains to concentrate on the outer cracks. On such conditions the strain gauge would only reproduce thermal strains induced by the daily temperature variations, as was effectively observed. These kinds of experimental difficulties, related to the inadequacy of the sensors usually adopted for hardened concrete to properly measure strains during the early ages (they are highly dependent on the efficiency of bond between the concrete and the sensor, which is negligible when the hydration reaction starts), points to the urgent need of a new generation of strain sensors suitable for this kind of applications, namely based on optical fibre technology [40].

5. Conclusions

A methodology for the thermo-mechanical analysis of concrete at early ages is presented, which accounts for the evolution of the cement hydration reaction and the inherent thermal and stress fields, providing a numerical tool to evaluate the cracking risk in practical structures. The thermal problem arising from the cement hydration reaction includes an Arrhenius law for the internal heat source, and it is solved adopting a FE spatial discretization and a backward-Euler time integration scheme. By computing a state variable called hydration degree the mechanical properties of concrete are easily updated during hydration, via explicit laws based on the current value of that variable. The mechanical problem that arises from the non-uniform thermal field is solved by the FE method, taking into consideration the changes in the mechanical properties of concrete due to ageing, and the creep and shrinkage phenomena.

The described numerical methodology was applied to a restrained RC slab monitored during construction. Combining two simple models, a 1D one for the thermal analysis across the thickness and a 2D one for the in-plane mechanical analysis of the slab, fairly good results were obtained when compared to a 3D thermo-mechanical analysis. Importance of creep was emphasized, and the overall agreement of the numerical predictions of temperatures, strains and cracking patterns with the in situ measurements

in the slab served for validating the models and assumptions outlined in the paper.

Acknowledgements

Financial support from the Portuguese Foundation for Science and Technology, through the PhD grant SFRH/BD/13137/2003, is gratefully acknowledged by the second author.

References

- [1] Sule M. Effect of reinforcement on early-age cracking in high strength concrete. PhD thesis, Delft, 2003.
- [2] De Schutter G. Finite element simulation of thermal cracking in massive hardening concrete elements using degree of hydration based material laws. *Comput Struct* 2002;80(27–30):2035–42.
- [3] Breugel K, Lura P. Deformational behaviour and self induced stresses in hardening concrete. IPACS document, Subtask 3.2, 2001.
- [4] Emborg M, Bernander S. Assessment of risk of thermal cracking in hardening concrete. *ASCE-J Struct Eng* 1994;120(10):2893–912.
- [5] Gutsch A. Crack control for the massive concrete structures of the new central railway station in Berlin, Germany. International workshop on control of cracking in early age concrete, Sendai, Japan, 2002.
- [6] Jonasson J-E. Modelling of temperature, moisture and stresses in young concrete. PhD thesis, Lulea University of Technology, Lulea, 1994.
- [7] Ulm F, Coussy O. Modeling of thermochemomechanical couplings of concrete at early ages. *J Eng Mech Div ASCE* 1995;121(7):785–94.
- [8] de Borst R, van den Boogaard A. Finite-element modeling of deformation and cracking in early-age concrete. *J Eng Mech Div ASCE* 1994;120(12):2519–34.
- [9] Zarr R. A history of testing heat insulators at the National Institute of Standards and Technology. In: ASHRAE Transactions 2001, NIST, 2001.
- [10] Morabito P. Thermal properties of concrete. Variations with the temperature and during the hydration phase. IPACS document, Subtask 2.3, 2001.
- [11] Lura P, Breugel K. Thermal properties of concrete: sensitivity studies. IPACS document, Subtask 2.5, 2001.
- [12] Breugel K. Prediction of temperature development in hardening concrete. Prevention of thermal cracking in concrete at early ages. Report 15, R. Springenschmid, E&FN SPON, 1998.
- [13] Ruiz J, Schindler A, Rasmussen R, Kim P, Chang G. Concrete temperature modeling and strength prediction using maturity concepts in the FHWA HIPERPAV software. In: 7th international conference on concrete pavements, Orlando (FL), USA, 2001.
- [14] Breugel K. Simulation of hydration and formation of structure in hardening cement-based materials. PhD thesis, Delft, 1991.
- [15] De Schutter G. Thermal properties. Early age cracking in cementitious systems. Report 25, A. Bentur, RILEM Publications s.a.r.l., 2001, p. 121–6.
- [16] Breugel K. Artificial cooling of hardening concrete. Concrete structures. Delft: Delft University of Technology; 1980.
- [17] Silveira A. The influence of thermal solicitations on the behaviour of reinforced concrete bridges. PhD thesis, LNEC, Lisbon, 1996 [in Portuguese].
- [18] Reinhardt H, Blaauwendraad J, Jongedijk J. Temperature development in concrete structures taking account of state dependent properties. In: International conference concrete at early ages, Paris, France, 1982.
- [19] Morabito P. Methods to determine the heat of hydration of concrete. Prevention of thermal cracking in concrete at early ages. Report 15, R. Springenschmid, E&FN SPON, 1998.

- [20] Wadsö L. An experimental comparison between isothermal calorimetry, semi-adiabatic calorimetry and solution calorimetry for the study of cement hydration. Nordtest report TR 522, 2003.
- [21] Maekawa K, Chaube R, Kishi T. Modelling of concrete performance. E&FN Spon; 1999.
- [22] Bentz D. Three-dimensional computer simulation of Portland cement hydration and microstructure development. *J Am Ceram Soc* 1997; 80(1).
- [23] D'Aloia L. Early age kinetics: activation energy, maturity and equivalent age. Early age cracking in cementitious systems. Report 25, A. Bentur, RILEM Publications s.a.r.l., 2001, p. 127–48.
- [24] Chengju G. Maturity of concrete: method for predicting early-stage strength. *ACI Mater J* 1989;86(4):341–53.
- [25] Incropera FP, DeWitt DP. Introduction to heat transfer. New York: John Wiley & Sons, Inc; 2001.
- [26] Branco F, Mendes P, Mirambell E. Heat of hydration effects in concrete structures. *ACI Mater J* 1992;89(2):139–45.
- [27] Breugel K, Koenders E. Solar radiation. Effect of solar radiation on the risk of cracking in young concrete. IPACS Document, Subtask 4.2, 2001.
- [28] Cervera M, Faria R, Oliver J, Prato T. Numerical modelling of concrete curing, regarding hydration and temperature phenomena. *Comput Struct* 2002;80(18–19):1511–21.
- [29] Larson M. Thermal crack estimation in early age concrete. Models and methods for practical application. PhD thesis, Lulea, 2003.
- [30] FIB. Structural concrete-Textbook on behaviour, design and performance updated knowledge of the CEB/FIP Model Code 1990, vol. 1, FIB-CEB/FIP; 1999.
- [31] Bentur A. Terminology and definitions. Early age cracking in cementitious systems. Report 25, A. Bentur, RILEM Publications s.a.r.l., 2001, p. 13–5.
- [32] Weiss J. Experimental determination of the ‘time zero’ t_0 (maturity-zero M_0). Early age cracking in cementitious systems, A. Bentur, RILEM Publications s.a.r.l., 2001, p. 195–206.
- [33] Krauß M, Hairiri K, Rostásy F. Non-destructive assessment of mechanical properties of concrete at very early ages by US techniques – Method, results and modelling. IPACS Document, Task 2 (T2.1/T2.2), 2001.
- [34] Rostásy F, Gutsch A, Krauß M. Computation of stresses and cracking criteria for early age concrete – methods of iBMB. IPACS Document, Task 3, 2001.
- [35] Bentz D, Lura P, Roberts J. Mixture proportioning for internal curing. *Concr Int* 2005;27(2):35–40.
- [36] PR EN 1992-1 (Final Draft) European Standard Eurocode 2: Design of concrete structures-part 1: general rules and rules for building, 2001.
- [37] Atrushi D. Tensile and compressive creep of early age concrete: testing and modelling. PhD thesis, Norwegian University of Science and Technology, Trondheim, Norway, 2003.
- [38] Bazant Z, Osman E. Double power law for basic creep of concrete. *Mater Struct, Research and Testing* 1976;9(49):3–11.
- [39] Azenha M. Behaviour of concrete at early ages. Phenomenology and thermo-mechanical analysis. MSc Thesis, Faculty of Engineering of Porto, 2004 [in Portuguese].
- [40] Glisic B, Simon N. Monitoring of concrete at very early age using stiff SOFO sensor. *Cement Concr Compos* 2000;22(2):115–9.